Quantum Electronics **48** (10) 880–885 (2018)

https://doi.org/10.1070/QEL16795

Superconducting qubits in Russia

I.S. Besedin, G.P. Fedorov, A.Yu. Dmitriev, V.V. Ryazanov

Abstract. **Results of the two-year research in the framework of the first Russian project for superconducting qubits, supported by the Foundation for Advanced Research, Federal Agency on Atomic Energy, and the Ministry of Science and Higher Education of the Russian Federation, are presented. The main result is the demonstration of single-qubit quantum gate operations using several types of superconducting qubits with a coherence time of more than 1 μs. The project develops this breakthrough scientific and technical line of research in Russia, in fact, from scratch. The fabrication technology of submicron-scale superconducting tunnel junctions and various coherent quantum structures (qubits) based on them has been worked out; preparation and control of quantum states for such qubits, quantum tomography of prepared states, and realisation and precision control of single-qubit quantum gate operations are demonstrated.**

Keywords: *quantum computing, Josephson junctions, superconducting qubits, single-qubit gates.*

1. Introduction

The purpose of the three-year project 'Development of Quantum Computing Technologies Based on Superconducting Circuits and Structures' of the Foundation for Advanced Research is to implement the universal set of quantum gate operations (gates), demonstrate a possibility of solving rapidly brute-force and optimisation problems on this basis, and prepare multiqubit systems (quantum simulators) in order to simulate the materials science problems related to the Ising model for magnetic materials and the Hubbard model for strongly correlated electron systems. This project, guided by the state customer (Dukhov All-Russia Research Institute of Automatics (VNIIA), Federal Agency on Atomic Energy) actually consolidated all Russian research teams having experience in realisation and study of superconducting quantum coherent structures (superconducting qubits): the recently formed laboratories (headed by A. Ustinov and O. Astaf'ev) at the National University of Science and Technology MISIS and the Moscow Institute of Physics and Technology (MIPT); E. Il'ichev's team at the Novosibirsk State Technical University; and the laboratories in Chernogolovka at the Institute of Solid State Physics (ISSP) of the Russian Academy of Sciences and the Russian Quantum Center (RQC), headed by V. Ryazanov and A. Ustinov, respectively. The long-term experience of A. Ustinov, O. Astaf'ev, and E. Il'ichev in studying superconducting qubits at foreign laboratories, as well as the participation of the theoretical group headed by V. Pogosov (VNIIA) and researchers of the R&E Centre 'Functional Micro/Nanosystems' organised by the VNIIA and the Bauman Moscow State Technical University (BMSTU) and headed by A. Rodionov are of great importance for the successful realisation of the project.

I.S. Besedin National University of Science and Technology MISIS, Leninsky prosp. 4, 119991 Moscow, Russia;
G.P. Fedorov Moscow Institute of Physics and Technology (State University), Institutskiy per. 9, 141701 Dolgoprudnyi, Moscow region, Russia; Russian Quantum Center (RQC), ul. Novaya 100A, 143025 Skolkovo, Moscow, Russia;
A.Yu. Dmitriev Moscow Institute of Physics and Technology (State University), Institutskiy per. 9, 141701 Dolgoprudnyi, Moscow region, Russia;
V.V. Ryazanov Russian Quantum Center (RQC), ul. Novaya 100A, Skolkovo, 143025 Moscow, Russia; Institute of Solid State Physics, Russian Academy of Sciences, ul. Akad. Osip'yana 2, 142432 Chernogolovka, Moscow region, Russia; Dukhov All-Russia Research Institute of Automatics, Sushchevskaya ul. 22, 127055 Moscow, Russia; e-mail: ryazanov@issp.ac.ru

Received 31 July 2018
Kvantovaya Elektronika **48** (10) 880–885 (2018)
Translated by Yu.P. Sin'kov

2. Technology of superconducting structures and types of superconducting qubits

The basics of the technology of superconducting Josephson junctions, superconducting microwave transmission lines, and high-Q coplanar resonators, which is necessary for implementing qubits, are elaborated at the MIPT, RQC/ISSP, and MISIS technological clean rooms, with subsequent transfer of the technology for reproducible fabrication at the VNIIA/BMSTU technological centre. The main elements of superconducting quantum-coherent structures (qubits) are submicron-scale Josephson tunnel superconductor–insulator–superconductor (SIS) junctions of the Al–AlO_x–Al type (Fig. 1).

Superconducting tunnel junctions are fabricated using shadow deposition [1] through two-layer electron resist masks (prepared by electron lithography). To form a tunnel barrier of desired thickness, the lower aluminium S layer of the SIS junction is controllably oxidised directly in the chamber of a high-vacuum system. We worked out the technology of tunnel SIS junctions with lateral sizes of 100–500 nm, critical currents I_c in the range from 10 nA to 1 μA, and critical current densities in the range of 0.1–3 kA cm^{-2}. These parameters can be reproduced with a spread of no more than 10%. The critical current I_c is the maximum superconducting (nondissipative) current that can flow through the tunnel barrier of the SIS junction. The value of the superconducting current $I_s = I_c \sin\phi$ through a Josephson tunnel SIS junction is also

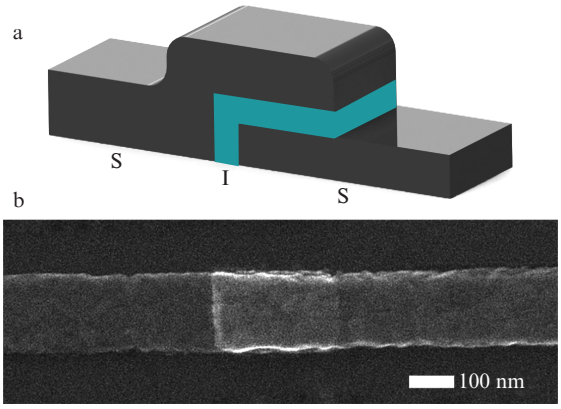

Figure 1. (a) Schematic and (b) microphotograph of a Josephson tunnel Al–AlO_x–Al junction.

characterised by the phase difference ϕ of the superconducting wave functions on the S layers of the SIS structure (see Fig. 1).

We also developed the technology of high-Q thin-film superconducting structures that are necessary for implementing superconducting qubit circuits: superconducting coplanar microwave transmission lines and resonators (Nb and Al), capacitors, air bridges, etc. Currently, the Q factor of the reproducibly fabricated coplanar resonators (with frequencies ranging from 5 to 10 GHz) exceeds 40 000.

A superconducting qubit [2] is characterised by two energies, which determine its Hamiltonian: the Josephson coupling energy $E_J = I_c\Phi_0/2\pi$, which is proportional to the critical superconducting current I_c through the tunnel junction (Φ_0 is a magnetic flux quantum), and the electric 'recharge' energy $E_c = (2e)^2/(2C_J)$ of a tunnel SIS structure (Fig. 1) with the capacitance C_J, related to the transfer of a superconducting electron (Cooper) pair with a charge $2e$ from one superconducting S layer of the tunnel junction to another. The charge (Q) and magnetic (ϕ) degrees of freedom of qubit are canonically conjugate variables, obeying the uncertainty relation $\Delta Q\Delta\phi \geqslant e$. If the energy E_c is comparable with the Josephson energy E_J or exceeds it, specifically the charge Q is a well-defined quantum-mechanical variable, and a qubit operating in this limit is referred to as a charge one. A charge qubit, which was implemented for the first time in 1999 [3], is strongly affected by the charge noise: the main source of decoherence, which significantly reduces the coherence time of superconducting qubit [4, 5]. Therefore, at the initial stage of the research in this field, preferred objects of study were phase [6] and flux [7] qubits, in which $E_J \gg E_c$ and the well-defined quantum-mechanical variable is the phase difference ϕ or magnetic flux Φ in a qubit.

A transmon [8] (a charge qubit shunted by a large external capacitance) turned out to be an ideal object in regards to combining the advantages of charge, phase, and flux qubits. As in the case of charge qubit, a transmon is characterised by a relatively small size of the Josephson junction (about 100 × 100 nm). The junction intrinsic capacitance is shunted by coplanar structures formed on the substrate surface. The substrate and the vacuum above the chip play the role of an insulator in the coplanar structures. In contrast to the amorphous tunnel barrier, consisting of disordered AlO_x, single-crystal substrate materials of high structural quality, such as high-resistance silicon or sapphire, have practically zero dielectric loss. Thus, the energy relaxation time in a transmon significantly exceeds that in charge qubits and is comparable with the photon lifetimes in coplanar resonators.

At the same time, shunting of this qubit by a large external capacitance, which significantly reduces the charge exchange energy E_c, makes the qubit weakly sensitive to charge noise, in contrast to phase and flux qubits with $E_J \gg E_c$. This statement can be illustrated by Fig. 2 (see also [8]). In Fig. 2a, which corresponds to the 'true charge' case with $E_J/E_c = 1$, the dependences of the qubit energy states E_i (i is the number of energy level) on the gate voltage (proportional to the induced normalised charge n_g) are parabolas. Each parabola corresponds to a charge state in which the difference in the numbers of pairs on the capacitor plates is $n = 0, \pm1, \pm2, \ldots$. The ground state energy minima are reached when the charge n_g is equal to n. Because of the pair tunnelling between S layers, parabolas with different n form quasi-intersections of levels with a splitting proportional to E_J.

Let us trace the evolution of the energy bands in Fig. 2 with an increase in the E_J/E_c ratio. At $E_J/E_c \gg 1$, the charge ceases to be a well-defined quantum-mechanical variable, and the dependence of the level energies on the gate voltage exponentially decreases. At $E_J/E_c = 100$ (Fig. 2b), the difference between energies of the ground and first excited states changes (depending on n_g) by no more than 10^{-7}.

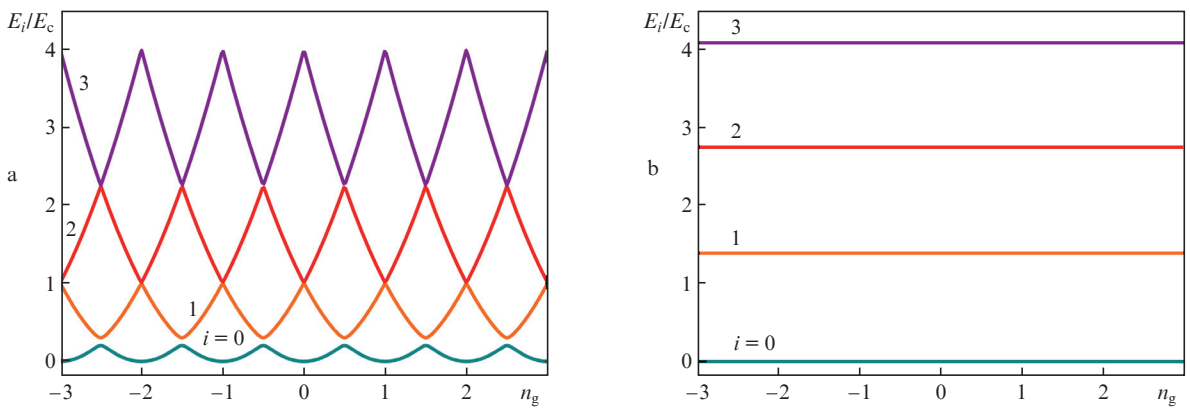

Figure 2. (Colour online) Calculated spectra of a charge qubit (transmon) at E_J/E_c = (a) 1 and (b) 100 [8].

Finally, a transmon often contains a two-contact superconducting quantum interference device (SQUID) rather than one Josephson junction. The transition energy of this qubit can be controlled using a magnetic flux. The dependence of the energy on magnetic field in the transmon is smoother than the similar dependences for the phase and flux qubits tunable by magnetic field, due to which the transmon is less sensitive to magnetic flux noise.

3. Low-temperature microwave techniques and qubit coherence times

Superconducting qubits are thin-film electric circuits with one or several Josephson junctions, having a sufficiently high Q factor and quantum transition frequencies lying in the microwave range (see, e.g., review [2]). The presence of a control line in qubit circuits allows one to adjust the qubit spectrum by an external magnetic field. The qubit working point is commonly reached by applying a magnetic flux through the qubit SQUID, whose value is close to half of magnetic flux quantum $\Phi_0/2$ (for flux qubit) or to Φ_0 (for transmons). In fact, a superconducting qubit is an 'artificial atom' realised on a substrate. A typical qubit spectrum, obtained by the participants of the project on a tunable transmon, is presented in Fig. 3.

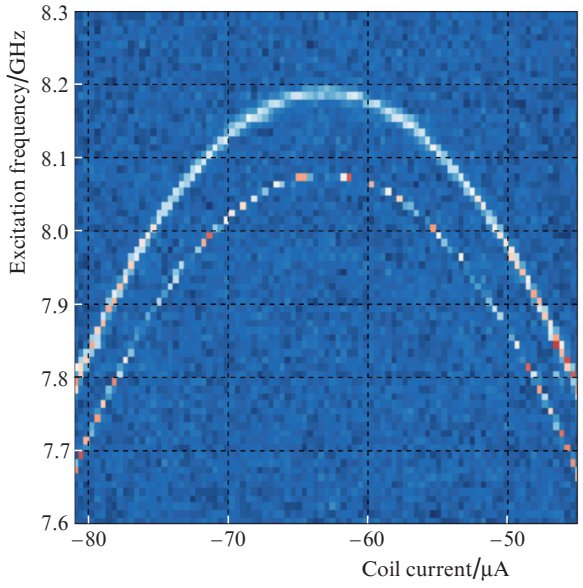

Figure 3. Spectrum of a superconducting qubit: (upper curve) the transition between the ground (|0⟩) and first excited (|1⟩) states and (lower curve) the two-photon transition |0⟩–|2⟩ as a function of the current through the coil creating the magnetic field applied to qubit SQUID.

The low frequencies of superconducting qubit quantum transitions (6–10 GHz) call for ultralow temperatures (below 50 mK) and the development of low-temperature microwave techniques. To manipulate with qubits and control their states, one also needs pulsed microwave techniques. Primarily, this is a measuring technique of Rabi oscillations, which are related to the transitions between the ground (|0⟩, or |g⟩) and excited (|1⟩, or |e⟩) qubit states under an applied microwave signal. Generally, the state of a qubit (quantum two-level system) is a superposition of |g⟩ and |e⟩ states: $\Psi = \alpha|g\rangle + \beta|e\rangle$. It is convenient to present it in the form of an arrow on the Bloch sphere (sphere with a unit radius and coordinate angles θ and φ) (Fig. 4).

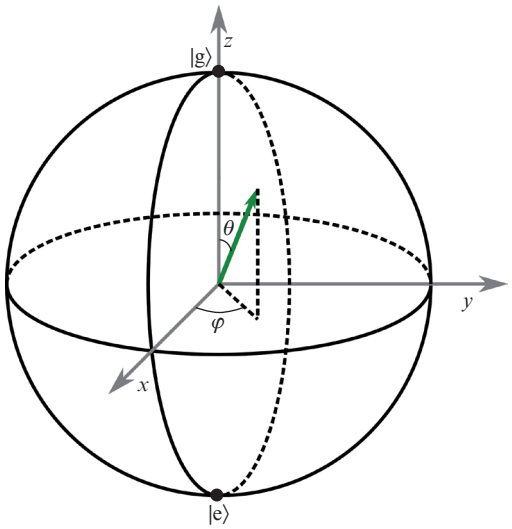

Figure 4. Qubit state on the Bloch sphere.

When applying a microwave signal at the qubit transition frequency, the arrow indicating the qubit state periodically moves between the basis states |g⟩ and |e⟩ and, depending on the excitation pulse duration Δt, finds itself at different points of the Bloch sphere. Rabi oscillations are used to calibrate the excitation pulse duration, primarily, for the π pulse (which transfers the qubit from the ground to excited state) and the π/2 pulse (transferring the qubit to the xy plane of the Bloch sphere). The qubit state is measured using the dispersion shift of the resonator coupled to the qubit with the shift values depending on the quibit state [9].

When designing superconducting qubits (artificial atoms on a substrate), the most important problem is to increase the qubit coherence time. To start working with two-cubit and multiqubit systems, which is planned by us for the end of 2018, it was necessary to reach coherence times exceeding 1 μs in the first stage. We investigated the two-island 3D (or 'cavity') transmons (Fig. 5a, on the right); 'planar' flux qubits (are not shown in Fig. 5); and, finally, the most popular 'planar' transmons (the so-called Xmon qubits [10]) (Fig. 5a, at the centre).

In the case of a two-island (cavity) transmon, which is a Josephson SIS junction shunted by a capacitance in the form of two thin-film pads located on the substrate at different sides from the SIS junction, measurements were performed using a cavity microwave resonator with a transmon qubit inside. The quantum states of the qubits of two other types (planar qubits) were read by coupling them to coplanar resonators on the substrate. A structure with six resonators coupled with qubits and connected to one microwave coplanar transmission line is shown in Fig. 5b. The key parameters in measurements were the energy relaxation times T_1 and phase relaxation times T_2^*. Figure 6 shows the measurement protocol and, as an example, the result of measuring the energy relaxation time T_1 for an Xmon qubit.

The average coherence times obtained in experiments with qubits of different types are listed in Table 1. These values are only estimates, because measurements were performed for specific qubit frequencies.

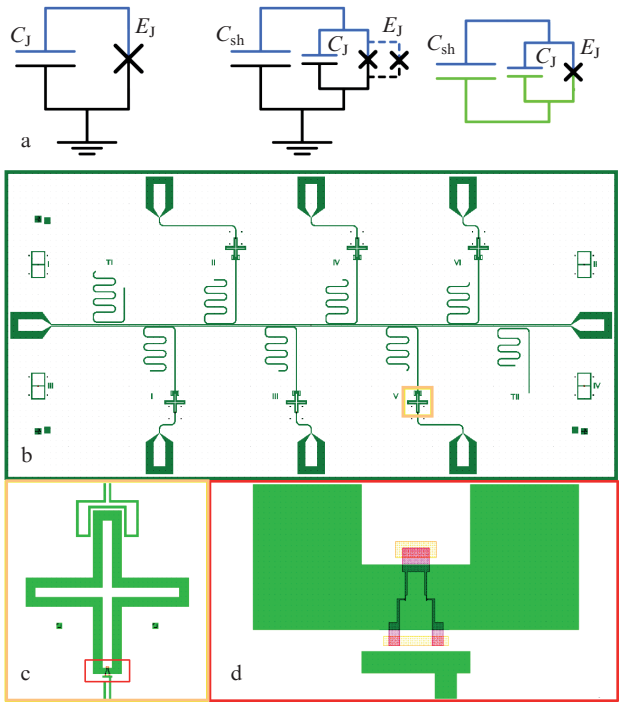

Figure 5. (Colour online) Equivalent circuits of qubits (from left to right): (a) charge qubit, Xmon qubit, and two-island transmon; (b) example of planar sample topology; (c) shunting capacitor for Xmon qubit with capacitance C_{sh}; and (d) microwave line for controlling the qubit frequency and Xmon SQUID.

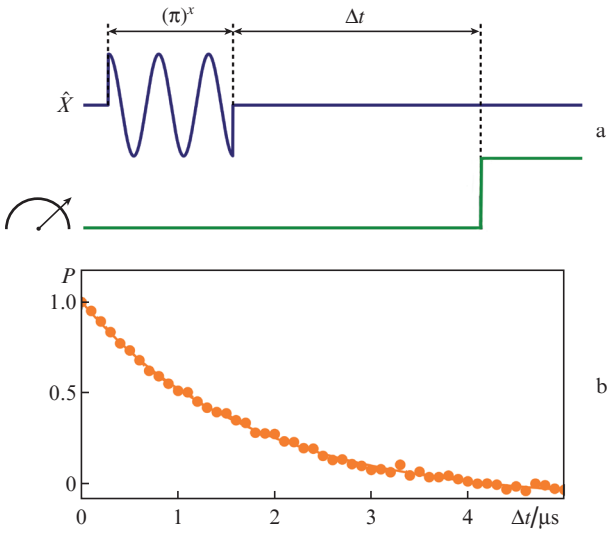

Figure 6. (a) Measurement protocol and (b) the relaxation of the excited state of Xmon qubit to the ground state with a characteristic decay time $T_1 = 1.74 \pm 0.04$ μs. The designation $(\pi)^x$ corresponds to the rotation of the qubit state vector by an angle π around the x axis. The upper signal ($\hat{X}$) is the microwave signal at the qubit frequency (control channel) and the lower signal is the microwave signal at the resonator frequency (reading channel); P is the excited state population.

The use of a shunting capacitance and a cavity resonator in the case of the 3D transmon made it possible to separate essentially the electromagnetic field from the main decoherence sources: two-level charge fluctuator defects, located in the amorphous oxide layers on the substrate near the qubit,

Table 1.

Qubit type	T_1/μs	T_2^*/μs
Flux qubit	~1.5	~1.5
Xmon	~2	~2.5
Bulk transmon	~3.6	~5

and, correspondingly, significantly increase the coherence time T_1.

To measure the second coherence time (phase relaxation time T_2^*), a π/2 pulse is first applied to a qubit to transfer its state onto the xy plane of the Bloch sphere and, after a time Δt, another π/2 pulse is applied (Fig. 7a); this sequence is necessary, because only the z component of the state on the Bloch sphere must be measured. When the difference $\Delta\omega$ between the pulse carrier frequency and the qubit frequency is small, the dependence of the excited state population P on Δt has the form of Ramsey beatings (or Ramsey 'fringes') [11], which are shown for an Xmon qubit in Fig. 7b. The longest time T_2^* was demonstrated for the 3D transmon, which is apparently related to the absence of superconducting loop (SQUID) in its structure; this circumstance leads to a significantly reduction of the magnetic noise influence, but, at the same time, considerably complicates the work with the 3D transmon (especially when the latter is used in multiqubit systems).

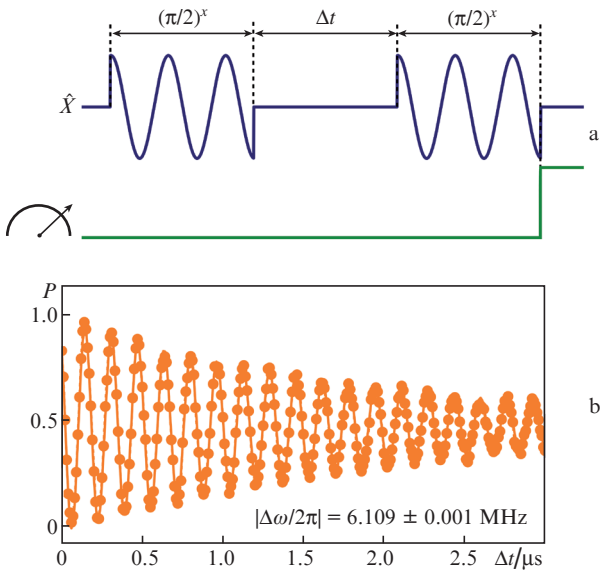

Figure 7. (a) Measurement protocol and (b) the phase relaxation of Xmon qubit with a characteristic time $T_2^* = 2.00 \pm 0.02$ μs. The designation $(\pi/2)^x$ corresponds to the rotation of the qubit state vector by an angle π/2 around the x axis.

Since the operations with multiqubit systems based on cavity 3D transmons (in a 3D waveguide) meet certain difficulties, most attention was paid to planar-type qubits, which are coupled with coplanar resonators located directly on the substrate. Figure 5b shows the topology of a structure containing a microwave line and six Xmon qubits coupled with resonators, each of which is a SQUID shunted by a capacitance [10]. The best coherence times obtained for Xmon qubits slightly exceeded 2 μs. The relatively low coherence times indicate that a qubit interacts with many

charge defects. It was observed for Xmon quibits by the leading world research groups that a decrease in the number of defects interacting with a qubit results in resonant coupling with only individual fluctuators or their small clusters, due to which the coherence time improved (increased) to 20 – 50 μs (see, e.g., [10]). However, the exponential relaxation observed by us gives grounds to believe that the planar structures under study approach the mode of the rarefied bath for two-level defects. To weaken the coupling between a qubit and fluctuators, one must further optimise the geometry of the system and improve the technological process in order to diminish the amorphous inclusions at the metal – substrate and substrate – vacuum interfaces. Optimisation of the geometry of the system should reduce the electric field strength in the regions characterised by low insulator quality (interfaces). In particular, we believe that it is important to increase the area of capacitor plates and widen the gap between them to this end. However, an increase in sizes, i.e., expansion of the region filled with electric field, may cause qubit coupling with spurious electromagnetic resonances; therefore, the presence of the latter should be minimised by efficient design of the samples and their holders.

4. Preparation of arbitrary states on the Bloch sphere and realisation of single-qubit gates

Along with the requirement of high qubit coherence, an important factor for using qubits as elements of a system of quantum data processing is the accurate control of its state by means of electromagnetic signals. The state preparation accuracy is measured by applying quantum tomography of states [12]. In the case of the radial tomography, after the preparation of a state using a microwave pulse, the state vector is rotated around different axes lying in the xy plane. Let us denote the angle between the rotation axis and x axis and the rotation angle as φ and Ω, respectively. The sequence of preparation and reading microwave signals, applied to a quantum system to carry out the state tomography, is shown in Fig. 8b.

Figure 8d shows the dependence of the excited state population P_{exp} on the amplitude and phase of the tomography pulse. The preparation pulse in this experiment corresponded to the rotation of the state vector by an angle of $\pi/4$ around the y axis and then by an angle of $\pi/3$ around the x axis on the Bloch sphere. The results were approximated using a theoretical model, whose parameters were taken to be the ele-

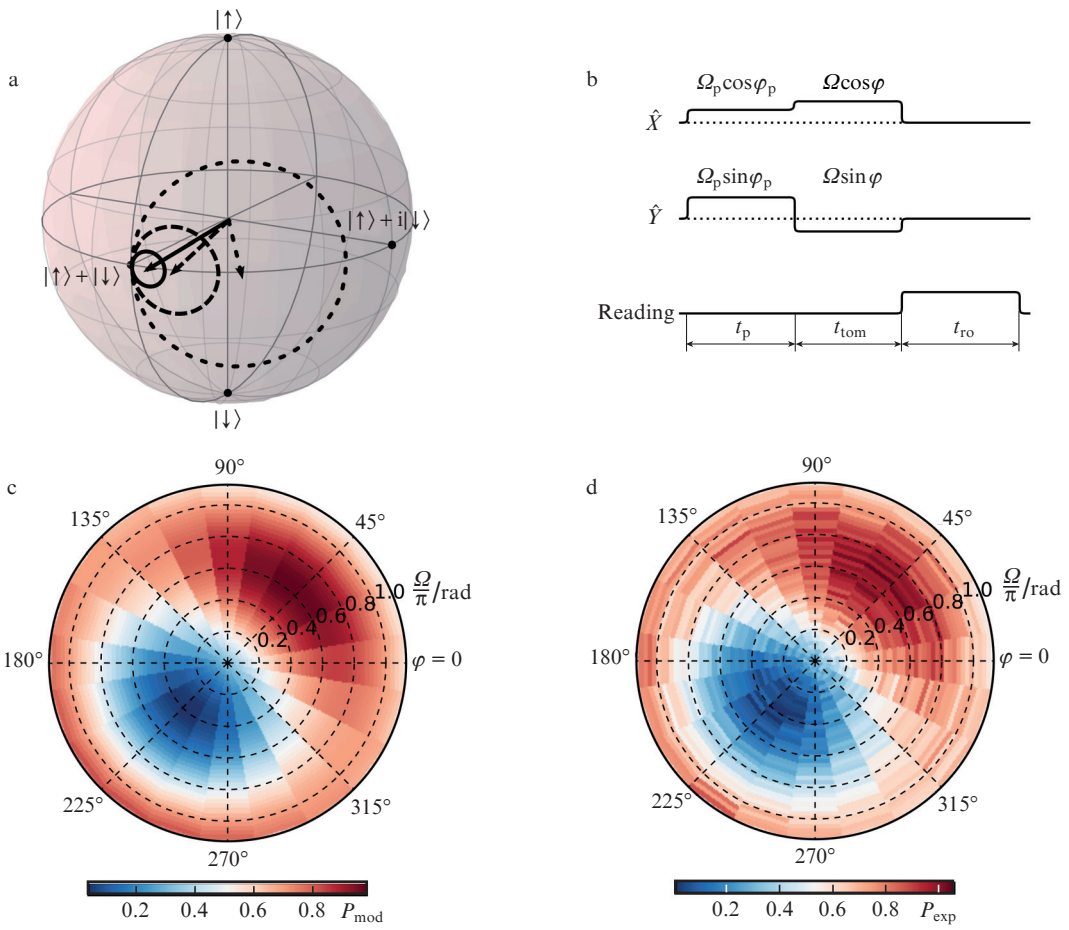

Figure 8. (Colour online) Radial tomography of qubit state: (a) state vector motion on the Bloch sphere; (b) sequence of microwave pulses for state preparation, vector state rotation in radial tomography, and reading; (c) approximation of the result using a theoretical model; and (d) experimental result of tomography of the state obtained via successive rotation of its vector by $\pi/4$ around the y axis and by $\pi/3$ around the x axis; Ω_p and φ_p are, respectively, the preparation pulse rotation angle and the angle between the x axis and the pulse rotation axis; Ω and φ are the same angles for a tomography pulse; $\hat{X}$ and $\hat{Y}$ are the microwave signal quadratures at the qubit frequency; and P_{mod} and P_{exp} are the populations of the excited qubit state.

ments of the density matrix $\hat{\rho}_m$ (Fig.8c). The gate performance accuracy F (fidelity) is calculated from the formula

$$F = \langle \psi_t | \hat{\rho}_m | \psi_t \rangle,$$

where ψ_t is the theoretical wave function. In the example presented in Fig. 8c, the state preparation accuracy for the chosen state of the Xmon qubit turned out to be 0.977.

Quantum gate operations (gates), corresponding to rotations by angles multiple of $\pi/2$ around three orthogonal axes (x, y, and z) of the Bloch sphere, play an important role in quantum data processing. These rotations form a Clifford group, which includes only 24 elements. The gate performance accuracy for transmon qubits in a bulk resonator was measured by randomised testing (benchmarking) [13]. This method makes it possible to measure precisely the gate performance accuracy in the presence of initialisation and qubit reading errors. All gates from the Clifford group C_i were performed using sequences with up to four pulses, which correspond to the rotations R_x and R_y around the x and y axes by angles of $\pi/2$. Microwave pulses are applied to a qubit in the ground state, which realise a random sequence of gates belonging to the Clifford group; a gate is performed in the end of each sequence, as a result of which the qubit is returned to the initial state, and reading is carried out. The result of measuring the transmon state in a bulk resonator in dependence of the number of gates from the Clifford group is shown in Fig. 9.

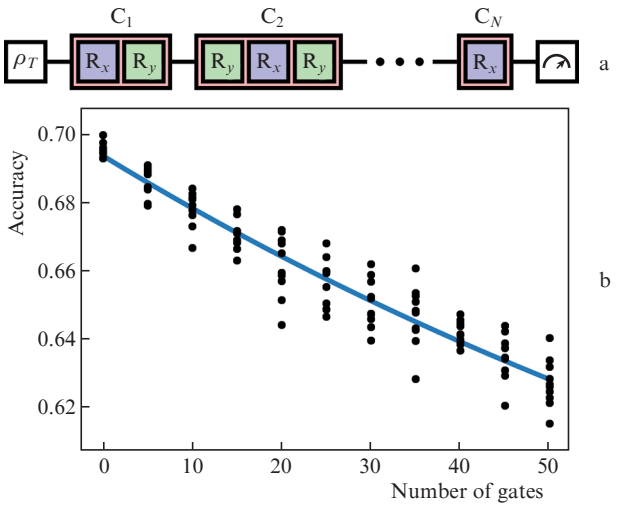

Figure 9. (a) Example of a random sequence of gates and (b) the result of measuring the gate performance accuracy. The solid line is an approximation; ρ_T is the initial qubit state.

The thus obtained dependence of the gate performance accuracy on their number was used to find the accuracy of qubit state preparation per gate: 0.995 ± 0.003. The low (0.69) accuracy in the absence of gates (Fig. 9) is related to the errors in qubit state initialisation and reading.

As was noted above, realisation of two-cubit systems (two-qubit gates) and multiqubit 'spin' chains is the goal of the second stage of the project (2018).

Acknowledgements. Successful execution of the project tasks was facilitated by the well-coordinated work of all organisations involved in the project (see Introduction). Along with the scientific leaders of the project (whose list should be supplemented with the names of I. Khrapach, V. Chichkov, and O.Vyaselev), we should especially note young researchers from the MIPT, MISIS, and ISSP RAS, as well as executors of the technological works performed at the BMSTU, MISIS, and MIPT under the guidance of I. Rodionov, V. Chichkov, and A. Bolgar, without whom the above-presented results could not be attained.

This work was supported by the Foundation for Advanced Research, Federal Agency on Atomic Energy, and the Ministry of Science and Higher Education of the Russian Federation.

References

1. Dolan G.J. *Appl. Phys. Lett.*, **34**, 337 (1977).
2. Clarke J., Wilhelm F.K. *Nature*, **453**, 1031 (2008).
3. Nakamura Y., Pashkin Y.A., Tsai J.S. *Nature*, **398**, 786 (1999).
4. Martinis J.M., Cooper K.B., McDermott R., Steffen M., Ansmann M., Osborn K.D., Cicak K., Seongshik Oh, Pappas D.P., Simmonds R.W., Clare C.Yu. *Phys. Rev. Lett.*, **95**, 210503 (2005).
5. Lisenfeld J., Bilmes A., Matityahu S., Zanker S., Marthaler M., Schechter M., Schön G., Shnirman A., Weiss G., Ustinov A.V. *Sci. Rep.*, **6**, 23786 (2016).
6. Martinis J.M., Nam S., Aumentado J., Urbina C. *Phys. Rev. Lett.*, **89**, 117901 (2002).
7. Van der Wal C.H., ter Haar A.C., Wilhelm F.K., Schouten R.N., Harmans C.J., Orlando T.P., et al. *Science*, **290**, 773 (2000).
8. Koch J., Yu T.M., Gambetta J., Houck A.A., Schuster D.I., Majer J., Blais A., Devoret M.H., Girvin S.M., Schoelkopf R.J. *Phys. Rev. A*, **76**, 042319 (2007).
9. Schuster D.I., Wallraff A., Blais A., Frunzio L., Huang R.-S., Majer J., Girvin S.M., Schoelkopf R.J. *Phys. Rev. Lett.*, **94**, 123602 (2005).
10. Barends R., Kelly J., Megrant A., Sank D., Jeffrey E., Chen Y., Yin Y., Chiaro B., Mutus J., Neill C., O'Malley P., Roushan P., Wenner J., White T.C., Cleland A.N., Martinis J.M. *Phys. Rev. Lett.*, **111**, 080502 (2013).
11. Ramsey N.F. *Phys. Rev. A*, **78**, 695 (1950).
12. Smithey D.T., Beck M., Raymer M.G., Faridani A. *Phys. Rev. Lett.*, **70**, 1244 (1993).
13. Knill E., Leibfried D., Reichle R., Britton J., Blakestad R.B., Jost J.D., Langer C., Ozeri R., Seidelin S., Wineland D.J. *Phys. Rev. A*, **77**, 012307 (2013).